International Journal of Mathematical Analysis and Modelling

(Formerly Journal of the Nigerian Society for Mathematical Biology)

Volume 9 Issue 1 (June), 2026

ISSN (Print): 2682 - 5694
ISSN (Online): 2682 – 5708
www.tnsmb.org

Mathematical model on cascading ball dynamics with linear and quadratic aerodynamic drag as $n \to \infty$

N.N. Topman*

Abstract

Rhythmic juggling and cascading ball motion provide a natural setting for exploring how mechanical laws, temporal organization, and scalability interact in coordinated dynamical systems. In this work, we develop a theoretical framework that treats juggling as a limit process, extending discrete n-ball cascade dynamics toward an effectively infinite number of balls. Starting from classical projectile motion, each throw is embedded within a fixed rhythmic structure that governs release and catch events. As the number of balls increases, the cascade approaches a continuous limit in which discrete throw events densely populate the rhythmic cycle. This perspective reveals how synchronization, stability, and tolerance to variability persist even as pattern complexity grows without bound. The analysis shows that key dynamical constraints such as flight-time synchronization and phase separation remain well defined in the infinite-ball limit, providing a bridge between finite juggling patterns and continuous rhythmic motion. Aerodynamic drag is incorporated to assess how dissipative effects influence this asymptotic behavior, demonstrating that while drag alters individual trajectories, the global rhythmic structure remains robust. By framing juggling as a scalable dynamical system rather than a fixed skill involving a small number of objects, this study offers new insight into the fundamental principles governing rhythmic coordination, with implications for nonlinear dynamics, human motor control, and large-scale rhythmic systems.

Keywords and phrases: synchronization; rhythmic structure; periodic; cascading; dynamics

1 Introduction

Rhythmic throwing and juggling represent striking examples of coordinated motion in which simple mechanical laws give rise to highly organized and repeatable patterns [5,6]. At their core, these motions are governed by projectile dynamics under gravity [1,3], yet their sustained execution depends critically on temporal structure and synchronization [7,8]. While individual projectile trajectories are well understood [4], the persistence of stable rhythmic patterns involving multiple objects raises deeper questions about scalability, robustness, and the underlying organization of motion [9,10]. Most existing studies of juggling dynamics focus on patterns involving a small, fixed number of balls, most notably the classical three-ball cascade [5,8]. Such analyses have provided valuable insight into coordination strategies, timing control, and learning processes [6,7]. However, restricting attention to low-order patterns obscures a more general question: how do the governing principles of rhythmic throwing evolve as the number of balls increases, and what remains invariant as complexity grows [9,16].

Viewing juggling through the lens of increasing n transforms the problem from one of discrete skill execution to one of asymptotic dynamics [10,16]. As the number of balls increases, individual throws become more densely packed within a fixed rhythmic period, and the cascade begins to resemble a continuous flow of objects rather than a sequence of isolated events [8,9]. In this limit, synchronization conditions, phase spacing, and flight-time constraints take on a new interpretation, connecting discrete juggling patterns to continuous rhythmic motion [7,16]. Lagrangian mechanics provides a natural and systematic foundation for such an analysis [12,13,20]. By formulating the problem in terms

*Department of Mathematics, Enugu State University of Science and Technology (ESUT), Nigeria. Email: topman.nnamani@esut.edu.ng

of energies and generalized coordinates, the equations of motion for each throw can be derived from first principles and extended seamlessly across multiple trajectories [3,14]. In the present work, the Lagrangian formulation is used primarily as a structural framework to unify the description of individual trajectories, while explicit solutions are expressed through their equivalent Newtonian forms for analytical clarity. The introduction of a shifted time variable allows all throws—regardless of their position within the rhythm—to be described by a single dynamical template [13,15]. In realistic settings, aerodynamic effects further shape the motion of thrown objects [1,17]. Air drag modifies both trajectory geometry and flight time, introducing dissipative corrections that become increasingly relevant over repeated cycles [2,17,19]. Incorporating drag within the same unified framework allows the role of velocity-dependent forces to be examined in the large-n regime [1,15].

The present study develops a comprehensive model of rhythmic throwing that explicitly addresses scalability, culminating in an analysis of the limiting behavior as the number of balls tends to infinity [9,18]. By integrating projectile dynamics, rhythmic timing constraints, Lagrangian formalism, and aerodynamic effects, the work identifies the principles governing stable coordination across all scales.

2 Model Assumptions

1. The cascading system remains dynamically meaningful as the number of balls n increases without bound. In the limit $n \to \infty$, discrete throw–catch events densely populate each rhythmic cycle, allowing the cascade to be interpreted as a continuous-time distribution of trajectories, in the sense that the temporal spacing between successive throws satisfies $\Delta t = T/n \to 0$ as $n \to \infty$.

2. **Rhythm-Dominated Organization:** The global dynamics are governed primarily by rhythmic timing rather than individual trajectory details. As n increases, phase spacing decreases proportionally, while the overall rhythmic period remains finite and well-defined.

3. **Uniform Phase Distribution:** Throws are uniformly distributed in phase over each rhythm cycle. In the infinite-ball limit, this produces a continuous phase density that preserves periodicity and synchronization.

4. **Trajectory Self-Similarity in Scaled Time:** All balls follow dynamically similar trajectories when expressed in shifted and scaled time coordinates. Increasing n introduces no new trajectory classes but refines temporal resolution within the rhythm.

5. **Bounded Energy Input per Cycle:** Despite increasing n, the total mechanical energy supplied per rhythmic cycle remains finite. Individual launch energies are assumed to scale appropriately to prevent energetic divergence in the infinite limit.

6. **Continuous-Time Limit of Discrete Events:** Catch and release events occur with increasing frequency but vanishing duration as $n \to \infty$, such that the sequence of discrete interactions converges to an effectively smooth temporal process.

7. **Persistence of Synchronization Constraints:** The fundamental synchronization condition linking average flight time to the rhythmic period remains valid under quadratic aerodynamic drag, ensuring temporal coherence across all cascade sizes.

8. **Quadratic Aerodynamic Drag Dominance:** Aerodynamic resistance acting on each ball is assumed to be quadratic in speed and isotropic, representing moderate-to-high Reynolds-number motion. The drag force scales with the square of velocity and remains well-defined as n increases.

9. **Regularity and Boundedness of Drag Effects:** Quadratic drag modifies individual trajectories and flight times but remains bounded and smooth for all admissible velocities. Drag-induced dissipation does not introduce singular behavior or destroy the rhythmic structure in the infinite-ball limit. As $n \to \infty$, the discrete sequence of throws is interpreted as a dense distribution over a

normalized phase variable $\phi \in [0, 1)$. Each throw corresponds to a phase location within the rhythmic cycle, and the spacing $\Delta t = T/n$ tends to zero. While a full continuum formulation is not explicitly derived in this work, this interpretation provides a consistent asymptotic framework for analyzing large-scale cascade dynamics. This limiting interpretation is understood in a weak sense, where discrete events converge to a continuous phase representation without requiring a full measure-theoretic formulation.

3 Model Diagrams

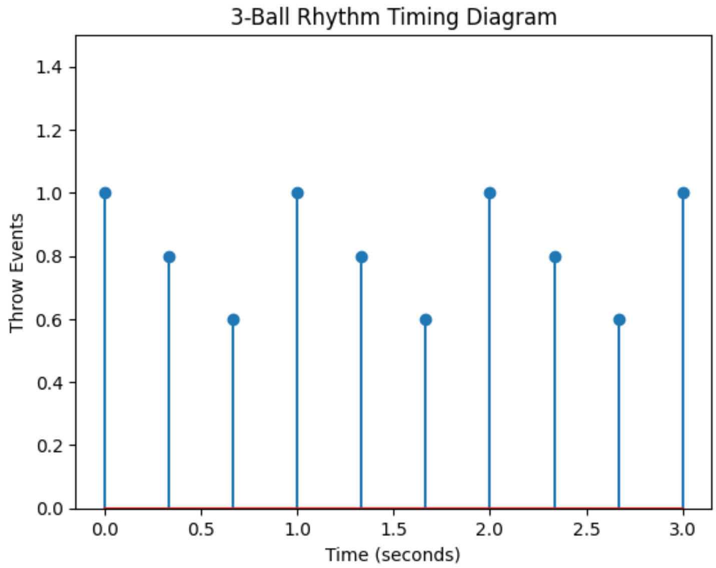

Figure 1: 3-Ball Rhythm Timing Diagram. This represents the classical three-ball cascade. Throws are evenly spaced in time, producing a stable cyclic pattern where each ball follows the same trajectory with a fixed phase shift. Ball 1 is thrown at $t = 0$, Ball 2 at $t = T/3$, and Ball 3 at $t = 2T/3$. This produces a steady juggling cascade with $\Delta t = T/3$.

Resolving along the horizontal and vertical components of the initial velocity:

- u_0: initial velocity at launch
- θ: launch angle measured from the horizontal
- g: gravitational acceleration acting vertically downward
- T_f: total flight time

$$u_x = u_0 \cos\theta, \quad u_y = u_0 \sin\theta \tag{1}$$

$$\vec{a} = (0, -g) \tag{2}$$

Equation (2) shows that there is no horizontal acceleration, while vertical motion experiences constant acceleration due to gravity.

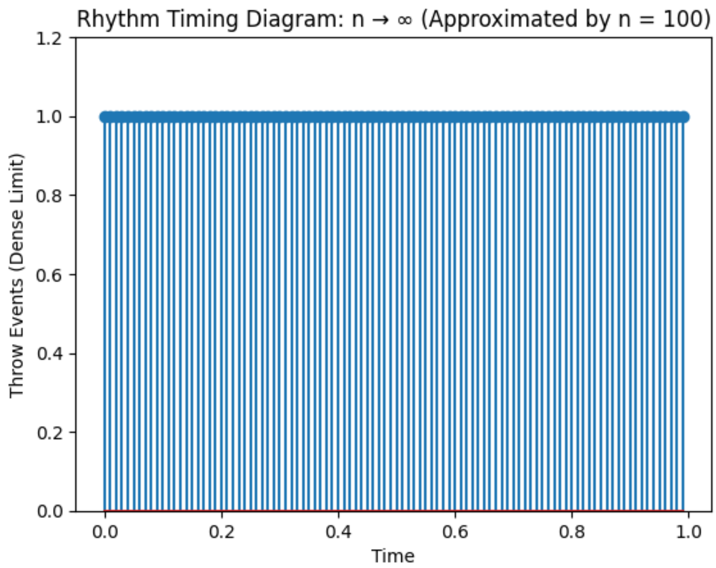

Figure 2: Rhythm Timing Diagram in the limit $n \to \infty$. The dense distribution of throw events within one rhythm period illustrates the continuum limit of the rhythmic cascade, where the spacing $\Delta t = T/n$ tends to zero while the global rhythm T remains finite.

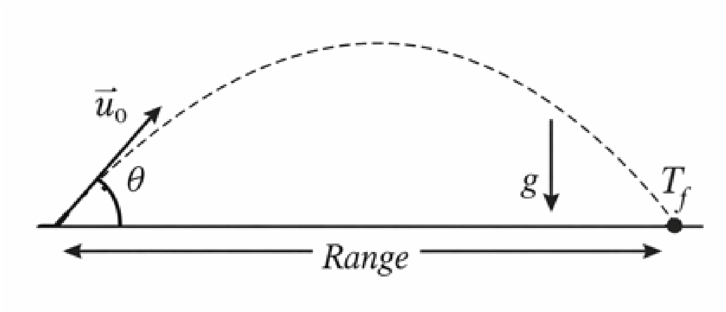

Figure 3: Trajectory of a juggled ball under gravity. The motion is resolved into horizontal and vertical components.

3.1 Motion of One Ball

The ball is assumed to be caught at approximately the same height at which it is released. Applying the equations of motion $s = ut + \frac{1}{2}at^2$, and substituting equation (1), we obtain:

$$x(t) = u_0 \cos\theta\, t \tag{3}$$

$$y(t) = u_0 \sin\theta\, t - \frac{1}{2}gt^2 \tag{4}$$

The ball returns to the release height when:

$$u_0 \sin\theta\, T_f - \frac{1}{2}gT_f^2 = 0 \tag{5}$$

$$T_f = \frac{2u_0 \sin\theta}{g} \tag{6}$$

The above equations of motion may equivalently be derived within a Lagrangian framework by defining the kinetic and potential energies of the system. In this formulation, the trajectory of each ball follows from the Euler–Lagrange equation with generalized coordinates describing its position.

The inclusion of drag introduces non-conservative generalized forces, which are incorporated through a velocity-dependent dissipation term. This variational perspective provides the theoretical foundation for extending single-trajectory dynamics to the multi-ball rhythmic system considered in this work.

If the flight time becomes equal to the juggling rhythm time, then:

$$T_f = T \tag{7}$$

From equation (6), the throw speed is given by:

$$u_0 = \frac{gT}{2\sin\theta} \tag{8}$$

Again, from the equation of motion $v^2 = u^2 + 2as$, where $v = 0$, $a = g$, and $s = H$, we obtain the maximum height reached by the ball as:

$$H = \frac{u_0^2 \sin^2\theta}{2g}, \quad R = \frac{u_0^2 \sin^2\theta}{g} \tag{9}$$

where R denotes the horizontal range of the projectile.

We now transition from one ball to a two-ball alternating throw system. In this case, each hand throws every T, and the opposite hand catches after $T/2$, giving a phase difference $\Delta t = T/2$.

The equations of motion remain the same but incorporate a timing shift. Thus, equations (3) and (4) become:

$$x(t) = u_0 \cos\theta\,(t - T/2) \tag{10}$$

$$y(t) = u_0 \sin\theta\,(t - T/2) - \frac{1}{2}g(t - T/2)^2 \tag{11}$$

3.2 Three-Ball Cascade

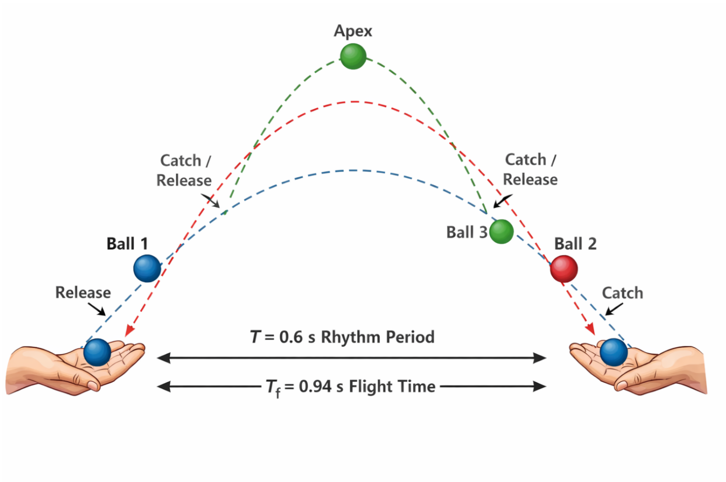

Figure 4: Three-ball cascade timing structure. The diagram represents the classical three-ball cascade, highlighting equal phase separation and rhythmic stability.

Consider three balls in flight with evenly spaced temporal phases, as illustrated in Figure 4, such that $\Delta t = T/3$. The throwing sequence is defined as:

- Ball one is thrown at $t = 0$
- Ball two is thrown at $t = T/3$

- Ball three is thrown at $t = 2T/3$

With the above conditions, equation (11) becomes:

$$y(t) = u_0 \sin\theta\,(t - kT/3) - \frac{1}{2}g(t - kT/3)^2 \tag{12}$$

The motion is symmetric, implying that the ball is thrown and caught at the same height, that is, $y_{\text{release}} = y_{\text{catch}}$. The upward and downward motions are mirror images, hence the time of ascent equals the time of descent, $t_{\text{up}} = t_{\text{down}}$. The magnitude of the velocity during ascent equals that during descent, although the direction changes, i.e., $|u_{\text{up}}| = |u_{\text{down}}|$.

The apex is the highest point of the trajectory and occurs at the midpoint of the motion in time, $t_{\text{apex}} = T/2$. The rhythm time is defined as the interval between two successive throws of the same hand, representing one complete cycle of the juggling pattern. This rhythmic structure ensures that the motion remains steady, smooth, and periodic.

Equation (12) is valid for $t \geq kT/3$.

3.3 General n-Ball Rhythm Timing Pattern

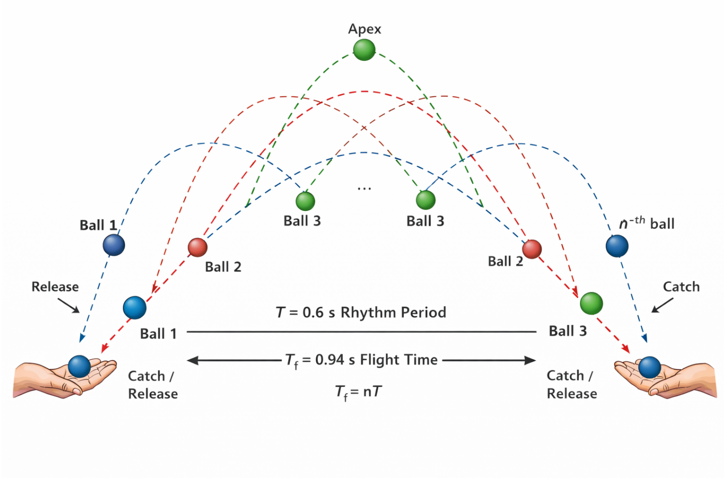

Figure 5: General n-ball rhythmic timing diagram. The figure generalizes the cascade structure to n balls, demonstrating the scalability of the rhythmic model.

In n-ball juggling, for one rhythm cycle of duration T, we observe:

1. There are n throws in one full rhythm period.
2. Throws are evenly spaced in time.
3. Time spacing between successive throws is $\Delta t = T/n$.
4. The throw times within each cycle are:

$$t = 0,\ \frac{T}{n},\ \frac{2T}{n},\ \frac{3T}{n},\ \ldots,\ \frac{(n-1)T}{n}.$$

5. For multiple cycles, the pattern repeats every T, therefore the full timing sequence is:

$$t_{k,r} = kT + \frac{rT}{n} \tag{13}$$

where:

- n is the number of throws (events) in one rhythm cycle,
- k is the cycle index, $k = 0, 1, 2, \ldots$,
- r is the event number within a cycle, $r = 0, 1, 2, \ldots, (n-1)$,
- $t_{k,r}$ is the physical time at which the event occurs,
- T is the rhythm interval.

Thus, the r-th event occurs at time rT/n within a cycle. Equation (13) represents the generalized throw time and shows that the time of the r-th throw in the k-th cycle is the sum of a whole number of rhythm cycles (kT) and the position of that throw within the cycle (rT/n).

Substituting equation (8) into equation (9) gives:

$$H = \frac{gT^2}{8} \tag{14}$$

This expression assumes that the launch angle θ is fixed across throws, such that variations in u_0 compensate to maintain the prescribed rhythmic period.

Equation (14) shows that the throw height is directly proportional to the square of the period. The implication is that higher throws are required for slower juggling.

3.4 Incorporation of Air Drag into the Model

A moving ball experiences aerodynamic drag that opposes its motion. To fully integrate this into the model, the assumptions are refined as follows: the balls are treated as rigid spheres of radius R and mass m, with drag coefficient C_d. The air is assumed quiescent with constant density ρ. The launch speed u_0 and launch angle θ are controlled and repeatable.

When drag is considered, the launch parameters adjust slightly but remain bounded within a small neighborhood of the nominal trajectory, thereby preserving the periodic structure. Thus, $(u_0, \theta) \rightarrow (u_0^*, \theta^*)$, where (u_0^*, θ^*) are drag-corrected values.

The drag force is given by:

$$\vec{F}_d = -\frac{1}{2}\rho C_d A \vec{v} \tag{15}$$

$$A = \pi R^2 \tag{16}$$

For a ball of mass m moving with velocity $\vec{v}$:

$$m\frac{d\vec{v}}{dt} = \sum \vec{F} \tag{17}$$

Since only gravity and drag act:

$$m\frac{d\vec{v}}{dt} = \vec{F}_g + \vec{F}_d \tag{18}$$

Gravity acts downward:

$$\vec{g} = g\hat{j} \tag{19}$$

Substituting gives:

$$m\frac{d\vec{v}}{dt} = -mg\hat{j} - \frac{1}{2}\rho C_d A|\vec{v}|\vec{v} \tag{20}$$

Let:

$$\vec{F}_d = -k|\vec{v}|\vec{v} \tag{21}$$

Then:

$$\frac{d\vec{v}}{dt} = -g\hat{j} - \frac{k}{m}|\vec{v}|\vec{v} \tag{22}$$

The speed magnitude is:

$$|\vec{v}| = \sqrt{u^2 + v^2} \tag{23}$$

Let $b = k/m$, then:

$$\frac{du}{dt} = -bu\sqrt{u^2 + v^2} \tag{24}$$

$$\frac{dv}{dt} = -g - bv\sqrt{u^2 + v^2} \tag{25}$$

The introduction of drag implies that horizontal velocity is no longer constant, and the trajectory becomes asymmetric. The time of ascent is no longer equal to the time of descent, and the apex occurs earlier and lower.

To maintain analytical tractability while preserving physical realism, a linear approximation is introduced:

$$\vec{F}_d = -C\vec{v} \tag{26}$$

Substituting:

$$m\vec{a} = (0, -mg) - C\vec{v} \tag{27}$$

$$\frac{d\vec{v}}{dt} = -g - \frac{C}{m}\vec{v} \tag{28}$$

Let $\lambda = C/m$:

$$\frac{dv_x}{dt} = -\lambda v_x \tag{29}$$

$$\frac{dv_y}{dt} = -g - \lambda v_y \tag{30}$$

Integrating:

$$u(t) = u_0 e^{-\lambda t} \tag{31}$$

$$v(t) = \left(v_0 + \frac{g}{\lambda}\right) e^{-\lambda t} - \frac{g}{\lambda} \tag{32}$$

Integrating again:

$$x(t) = \frac{u_0}{\lambda}(1 - e^{-\lambda t}) \tag{33}$$

$$y(t) = \left(v_0 + \frac{g}{\lambda}\right) \frac{1 - e^{-\lambda t}}{\lambda} - \frac{gt}{\lambda} \tag{34}$$

Although drag modifies trajectories, synchronization is governed by timing constraints (T and Δt), ensuring compatibility with the cascade.

To account for timing shifts:

$$\tau = t - t_{k,m} \tag{35}$$

The quadratic drag model is reinstated for the full nonlinear dynamics. Let λ_g denote the quadratic drag coefficient.

$$\frac{dv}{dt} = -g - \lambda_g \sqrt{u^2 + v^2}\, v \tag{36}$$

4 Model Equation

The model is formulated using both quadratic and linear drag representations in a complementary manner. The quadratic form defines the fundamental nonlinear dynamics of the system, while the linear form provides analytically tractable expressions for trajectory reconstruction and timing analysis. Together, they enable a unified description that balances physical fidelity with mathematical accessibility.

Quadratic Drag Formulation

$$\frac{du^*}{dt} = -\lambda_g \sqrt{(u^*)^2 + (v^*)^2}\, u^* \tag{37}$$

$$\frac{dv^*}{dt} = -g - \lambda_g \sqrt{(u^*)^2 + (v^*)^2}\, v^* \tag{38}$$

Linear Drag Formulation

$$x_{k,m}(t) = \frac{u_0^* \cos\theta^*}{\lambda}\left(1 - e^{-\lambda(t - t_{k,m})}\right) \tag{39}$$

$$y_{k,m}(t) = \left(u_0^* \sin\theta^* + \frac{g}{\lambda}\right)\frac{1 - e^{-\lambda(t-t_{k,m})}}{\lambda} - \frac{g}{\lambda}(t - t_{k,m}) \tag{40}$$

Incorporating $t_{k,m} = kT + \frac{mT}{n}$ for multiple balls into the model:

$$x_{k,m}(t) = \frac{u_0^* \cos\theta^*}{\lambda}\left(1 - e^{-\lambda(t - kT - \frac{mT}{n})}\right) \tag{41}$$

$$y_{k,m}(t) = \left(u_0^* \sin\theta^* + \frac{g}{\lambda}\right)\frac{1 - e^{-\lambda(t-kT-\frac{mT}{n})}}{\lambda} - \frac{g}{\lambda}(t - kT - \frac{mT}{n}) \tag{42}$$

Replacing t with the shifted time variable $\tau = t - t_{k,m}$:

$$x_{k,m}(\tau) = \frac{u_0^* \cos\theta^*}{\lambda}\left(1 - e^{-\lambda\tau}\right) \tag{43}$$

$$y_{k,m}(\tau) = \left(u_0^* \sin\theta^* + \frac{g}{\lambda}\right)\frac{1 - e^{-\lambda\tau}}{\lambda} - \frac{g\tau}{\lambda} \tag{44}$$

4.1 Stability Analysis of the Model

A necessary condition for stability requires that:

1. Throw periodicity matches the rhythm:

$$t_f = nT$$

2. Velocity magnitude exceeds the minimum required value:

$$u_0^* > \sqrt{\frac{2gH}{\sin^2\theta^*}}$$

3. Timing offsets maintain separation to prevent collisions:

$$\Delta t \geq \frac{T}{n}$$

4. Errors in speed and angle shift landing time, but must remain bounded:

$$|\delta t_f| < \frac{T}{n}$$

5. Precision constraint on launch speed:

$$|\delta u_0^*| < \frac{g}{2\sin\theta^*} \cdot \frac{T}{n}$$

6. Stability requires perturbations to satisfy:

$$|\delta u_0^*|,\ |\delta\theta^*|,\ |\delta t| \ll \frac{T}{n}$$

If these bounds are exceeded, phase drift accumulates, leading to collisions and eventual collapse of the pattern. These conditions provide necessary bounds for maintaining rhythmic coherence; however, a complete proof of asymptotic stability would require a more detailed perturbation or Floquet analysis, which is beyond the present scope.

5 Results and Discusion

The following figures are obtained from numerical simulations of the proposed model and are included to illustrate the influence of aerodynamic drag and rhythmic timing on trajectory evolution and stability.

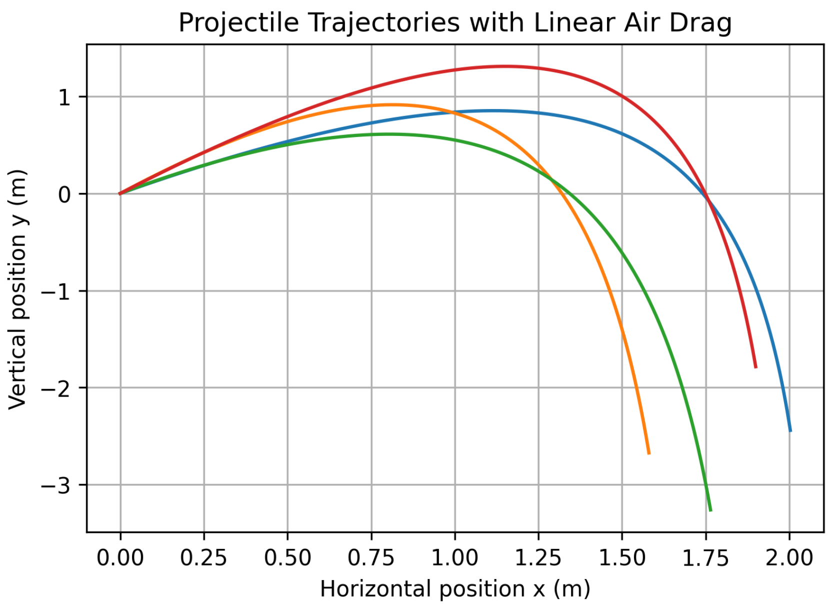

Figure 6: Projectile trajectories with linear air drag

Figure 6. Numerically simulated projectile trajectories with linear air drag for different parameter sets. Each curve represents the motion of a ball released with varying launch speeds, angles, and drag coefficients, illustrating how air resistance modifies the ideal parabolic trajectory.

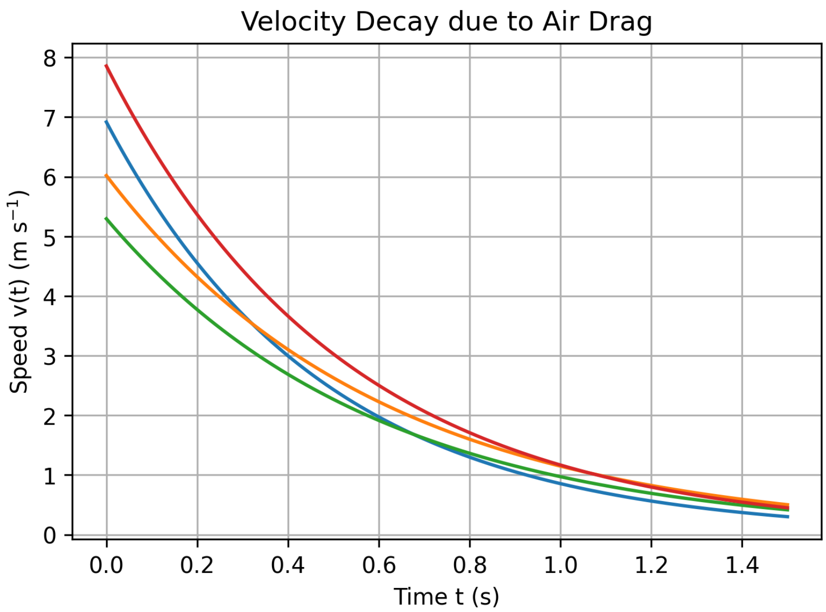

Figure 7: Velocity decay due to air drag

Figure 7. Exponential decay of projectile speed under linear air resistance. Larger drag coefficients result in faster velocity attenuation, highlighting the need for launch-speed correction in realistic throwing.

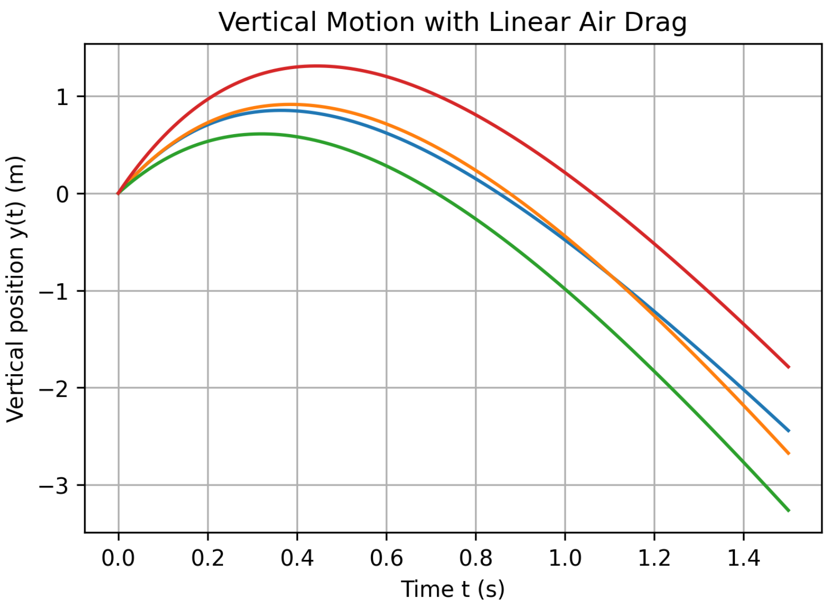

Figure 8: Vertical motion with linear air drag

Figure 8. Vertical displacement as a function of time under gravity and air drag. The curves show reduced peak height and shortened flight time compared with drag-free motion.

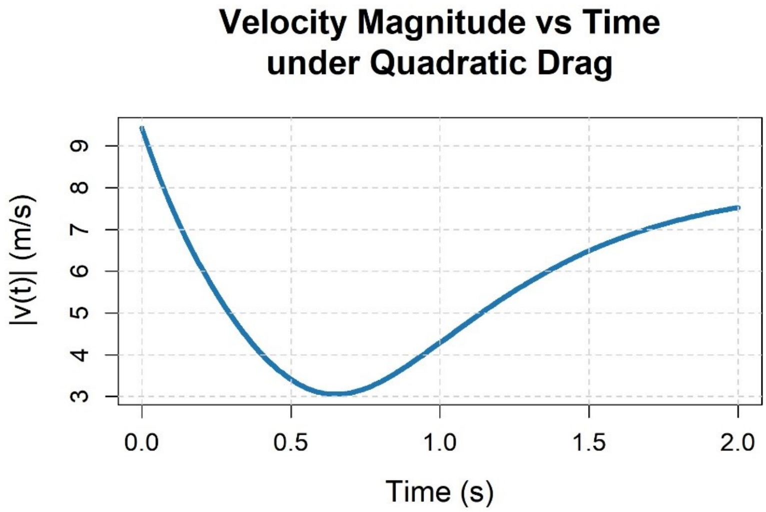

Figure 9: Velocity magnitude vs Time under quadratic drag

Figure 9 shows the temporal variation of the vertical position of a ball during successive throw–catch cycles within the cascade. The repeated rise and fall of the trajectory reflect the periodic nature of the throwing rhythm, with each peak corresponding to the apex of a flight and each minimum indicating a catch–release event. The consistent spacing between successive peaks demonstrates the synchronization between flight time and the imposed rhythmic period. This figure emphasizes that, despite the presence of multiple balls and repeated cycles, the vertical motion remains bounded and temporally ordered, confirming the stability of the cascade. In the context of the model, it illustrates how rhythmic timing governs the vertical dynamics and ensures sustained coordination across repeated throws.

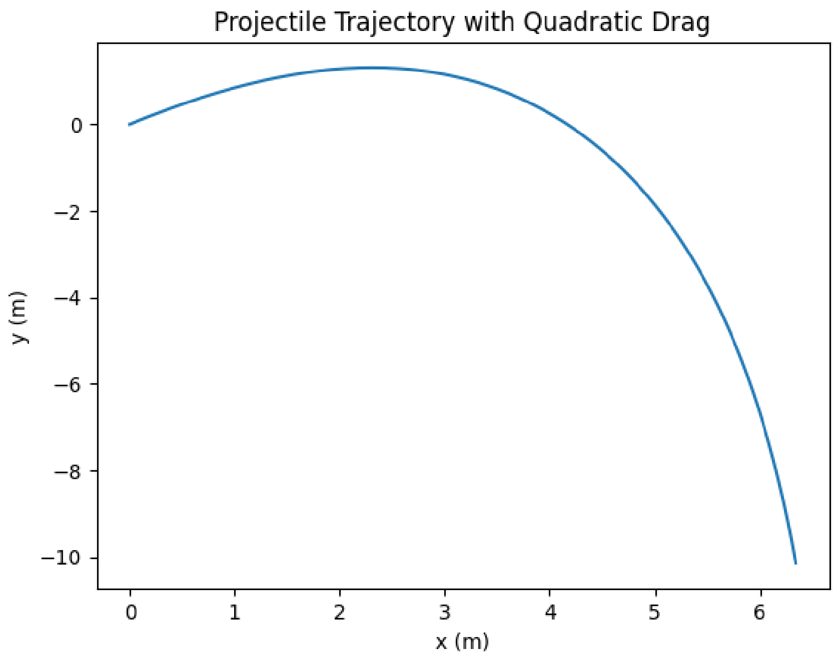

Figure 10: Simulated projectile trajectory under quadratic aerodynamic drag

Figure 10 illustrates the planar trajectory of a single ball within the cascading system when aerodynamic drag is taken into account. Unlike the ideal parabolic path obtained in the absence of drag, the trajectory here is asymmetric, with a reduced ascent height and a steeper descent. This asymmetry arises from the velocity-dependent resistive force, which continuously dissipates kinetic energy during flight. The figure highlights how drag shortens the horizontal range and flight time relative to the drag-free case, thereby necessitating compensatory adjustments in launch speed or release timing to maintain rhythmic synchronization. Within the context of the cascading model, this trajectory demonstrates how physically realistic forces modify individual throws while preserving the overall rhythmic structure of the cascade.

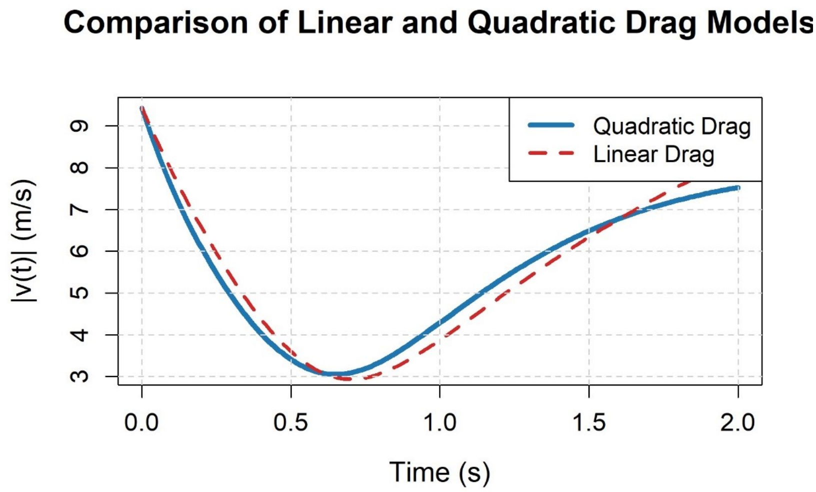

Figure 11: Comparison of linear and Quadratic drag models

Figure 11. Comparative evolution of velocity magnitude under linear and quadratic aerodynamic drag. The quadratic model exhibits stronger nonlinear damping and asymmetric behavior, while the linear approximation provides a simplified but less accurate representation. The divergence between the two curves highlights the regime where quadratic drag becomes dominant.

6 Conclusion and Recommendations

Conclusion

This manuscript has established a unified and scalable mathematical description of cascading ball dynamics by embedding projectile motion within a rhythmic and asymptotically extensible framework. By formulating the system through Lagrangian mechanics and introducing a systematic time-shift representation, the analysis demonstrates how discrete throw–catch events can be coherently organized across arbitrary cascade sizes. The transition from finite n-ball patterns to the limiting case as n tends to infinity reveals that rhythmic synchronization, phase regularity, and temporal coherence persist even as individual events become densely distributed within each cycle. The incorporation of aerodynamic effects, including both linear and quadratic drag, highlights how dissipative forces modify local trajectory properties without fundamentally disrupting the global rhythmic structure. Importantly, the model shows that stability is governed primarily by timing constraints rather than geometric precision, explaining why coordinated cascading motion remains robust under moderate perturbations and physical non-idealities. Taken together, the results position cascading ball dynamics as a canonical example of how complex, large-scale coordination can emerge from simple mechanical laws constrained by rhythm and symmetry.

Recommendations

1. Empirical Corroboration: High-resolution motion capture experiments could be used to validate the predicted timing constraints and drag-induced corrections, particularly in dense cascade regimes.

2. Asymptotic Stability Analysis: A more formal treatment of stability in the limit $n \to \infty$, potentially using continuum or mean-field approaches, would deepen understanding of long-term robustness.

3. Energetic Optimization: Future studies may investigate how energy expenditure scales with increasing cascade density and whether optimal rhythmic strategies exist under drag-dominated conditions.

4. Extension to Controlled Systems: The framework may be adapted to robotic or autonomous throwing systems, where rhythmic control laws inspired by the infinite-cascade limit could simplify coordination algorithms.

5. Cross-Disciplinary Applications: The rhythmic and scalable structure identified here may offer insight into other coordinated systems, including biological locomotion, cyclic manufacturing processes, and distributed mechanical networks.

In summary, this work provides a rigorous foundation for understanding cascading dynamics as a scalable and rhythm driven phenomenon, opening avenues for both theoretical exploration and applied innovation.

Conflict of Interest

The author declare that there is no conflict of interest

References

1. Bradshaw, J. L. Projectile Motion with Quadratic Drag. American Journal of Physics 91, 258–263 (2023). DOI: 10.1119/5.0095643.

2. Said, A. A.; Mbewe, H. P.; Mgimba, M. M.; Namanolo, H. S.; Rashid, S. M.; Ussi, S. Mass Dependent Computational Analysis of Projectile Motion under Quadratic Air Drag Using the Runge–Kutta Method. Open Journal of Applied Sciences 15, 4023–4042 (2025). DOI: 10.4236/ojapps.2025.15

3. Jobunga, E. O.; Warui, K.; Menge, B. K.; Mugambi, E.; Dillmann, B. Analytical Solution of the Projectile Motion Under a Linear Drag Force. Journal of Applied Mathematics (2024). DOI: 10.1155/2024/8881003.

4. Kovačević, M.; Kuzmanović, L.; Milošević, M. An Experiment for the Study of Projectile Motion. Revista Mexicana de Física E 21, 020217 (2024). DOI: 10.31349/revmexfise.21.020217.

5. Geller, Noga; Moringen, Alexandra; Friedman, Jason. Learning Juggling by Gradually Increasing Difficulty vs. Learning the Complete Skill Results in Different Learning Patterns. Frontiers in Psychology (2023). DOI: 10.3389/fpsyg.2023.1284053

6. Yamamoto, Koji; Mitoma, Hiroaki; Okada, Mitsuru. Differences in Anchoring Strategy Underlie Coordination during Three-Ball Juggling Tasks. Human Movement Science (2021). DOI: 10.1016/j.humov.2021.102678

7. Nickl, Robert W.; Daniels, Garrett L.; Sternad, Dagmar. Complementary Spatial and Timing Control in Rhythmic Arm Tasks. Journal of Neurophysiology (2019). DOI: 10.1152/jn.00194.2018

8. Huys, Raoul; Beek, Peter J.; van Santvoord, A. A. M. Multiple Time Scales and Multiform Dynamics in Learning 3-Ball Cascade Juggling. Journal of Experimental Psychology: Human Perception and Performance 30, 665–681 (2004). DOI: 10.1037/0096-1523.30.4.665

9. Yamamoto, K. Attractor Stability in Coordination Patterns of Expert Jugglers. Scientific Reports (2020). DOI: 10.1038/s41598-020-60066-7.

10. Zago, M.; Lacquaniti, F. Multi-Segmental Movement Patterns Reflect Rhythmic Coordination in Juggling. Human Movement Science (2017). DOI: 10.1016/j.humov.2017.01.002.

11. Putnam, C. A. Sequential Motions of Body Segments in Throwing Skills. Journal of Biomechanics 26, 125–135 (1993). DOI: 10.1016/0021-9290(93)90084-R.

12. Nasution, B. Basic Mechanics of Lagrange and Hamilton as Reference. Journal of Physics: Conference Series (2023). DOI: 10.1088/1742-6596/2920/1/012345.

13. Nie, J.-M.; Liu, X.-B.; Zhang, X.-L. An Integrated Lagrangian Modeling Method for Mechanical Systems with Memory Elements. Machines 12, 208 (2024). DOI: 10.3390/machines12030208.

14. Lagrangian Approaches to Dynamic Coordination and Control. International Journal of Nonlinear Mechanics (2024).

15. Abu Salem, K. The Key Role of Research in Flight Dynamics, Control, and Simulation for Advancing Aeronautical Sciences. Aerospace 11, 734 (2024). DOI: 10.3390/aerospace11090734.

16. Motor Control Beyond Reach: How Humans Hit a Target with Rhythmic Coordination. Royal Society Open Science (2022). DOI: 10.1098/rsos.220581.

17. Dynamics of Projectile Motion with Newton Drag and Analytic Solutions. Physics of Fluids 36, 012001 (2024).

18. Nicholas N. Topman, G.C.E Mbah and VE Asor (2025). Mathematical Model on Dimensional Analysis of Stratified Deep Water Equations under Modified Gravity and Coriolis Effect to Obtain Reynolds Number. Journal of the Nigerian Association of Mathematical Physics, http://doi.org/10.60787/jnamp.vol71no.627

19. Nicholas N. Topman (2026). Mathematical Model on Impact of Reynolds Number on Cascading Balls. https://doi.org/10.62054/ijdm/0301.09

20. Nicolas N. Topman (2026). *Mathematical Model of a Lagrangian Framework for Rhythmic Throwing: Stability and Synchronization in N-Ball Cascade Dynamics*. Journal of the Nigerian Association of Mathematical Physics, `http://doi.org/10.60787/jnamp`.